

Cite this: *RSC Adv.*, 2019, 9, 25142

Synthesis, growth mechanism and photocatalytic H₂ evolution of CdS/CuS composite via hydrothermal method

Xiande Yang,^{†ab} Guangwen Lu,^{†a} Boyou Wang,^a Tinglan Wang^a
and Yongqian Wang^{id*ac}

In recent years, visible light-driven photocatalysts used for confronting energy shortages and environmental pollution have drawn much attention. CdS is regarded as an excellent photoelectric semiconductor for photocatalysis, but photocorrosion and low photocatalytic activity limit its practical application. In order to improve the photocatalytic performance of CdS, we synthesized a II-type CdS/CuS composite via a hydrothermal method in one step. CdS, CuS and the CdS/CuS composite have flower-like structures according to FESEM results. XRD and EDS results confirm that the composite is composed of CdS and CuS, indicating that we have successfully synthesized the CdS/CuS composite. UV-Vis and PL results show that the formation of heterojunction structures with CuS can be used to control the optical properties of CdS. H₂ evolution results show that the CdS/CuS composite generates H₂ at a rate of 295 $\mu\text{mol g}^{-1} \text{h}^{-1}$, which is higher than that of CdS.

Received 10th June 2019
Accepted 24th July 2019

DOI: 10.1039/c9ra04336e

rsc.li/rsc-advances

1. Introduction

Energy consumption and environmental pollution have become a crisis due to the development of modern living standards; it is a challenge for us to find an efficient way to solve these problems.¹ In past research reports, hydrogen energy has been considered a sustainable and clean form of energy, and it can be abundantly obtained by splitting of water into hydrogen using nanomaterials, which is a promising and attractive strategy for confronting the above issues.^{2–4} Thus, various nanomaterials have been used as effective photocatalysts for splitting water to produce H₂, such as TiO₂,⁵ ZnO,⁶ g-C₃N₄,⁷ CuS⁸ and BiVO₄.⁹ In addition, photocatalytic H₂ evolution is critically related to the size, structure, surface area and morphology of the nanomaterials used.¹⁰ Therefore, various morphologies of nanomaterials have been reported, such as ZnO nanorods,¹¹ TiO₂ nanospheres,¹² MoS₂ nanosheets,¹³ and flower-like CdS structures.¹⁴ However, in the field of photocatalytic nanomaterials, the major challenge is to find efficient and stable nanomaterials for photocatalytic application under solar light.

Among these types of nanomaterials, CdS has attracted much attention due to its conduction band position and band gaps being suitable for energy conversion under visible light.¹⁵ As is known, CdS (2.42 eV) is an important visible light photocatalyst because of its sensitivity to visible light irradiation and efficient photoexciton generation, which are excellent qualities for a photocatalyst.^{16,17} However, CdS has some disadvantages for further application. First, CdS nanostructures can easily aggregate during photocatalytic reactions, which can reduce the surface area. Second, the photoexciton recombination is ultrafast, and there is a lack of reactive sites.¹⁸ Third, instability occurs due to photocorrosion or photodissolution.¹⁹ Therefore, CdS usually exhibits low photocatalytic activity due to the above drawbacks. To solve these problems, significant efforts have been devoted to improving the photocatalytic activity of CdS. Examples include the synthesis of CdS quantum dots with high surface areas,²⁰ deposition of noble metals,²¹ loading cocatalysts onto the CdS surface,²² metal ion doping,²³ and the incorporation with other semiconductors to form heterojunction structures.²⁴

In comparison with noble metal cocatalyst addition and metal ion doping, the hybridization of CdS with other semiconductors having matching band gaps to form heterojunction structures is beneficial for suppressing the recombination of photoinduced charge carriers. Furthermore, this approach can effectively improve spatial charge separation and prolong the lifetime of the charge carriers, which can enhance the photocatalytic properties.²⁵ In addition, this charge separation is better facilitated by a II-type system than a I-type system.²⁶ Therefore, we tried to synthesize a II-type CdS heterojunction

^aEngineering Research Center of Nano-Geomaterials of Ministry of Education, Faculty of Material Science and Chemistry, China University of Geosciences, 388 Lumo Road, Wuhan 430074, P. R. China. E-mail: cugwyq@126.com; Tel: +86 138-7137-9285

^bCollege of Chemistry and Material Science, Nanning Normal University, Nanning 530001, P. R. China

^cGuangdong Provincial Key Laboratory of Soil and Groundwater Pollution Control, Shenzhen 518055, P. R. China

[†] Co-first author.



structure in one step to enhance the photocatalytic activity. CuS is an important semiconductor due to its excellent physical and chemical properties with a band gap of about 2.0 eV, with potential applications in photocatalysis, photothermal conversion, and solar cells.²⁷ Markovskaya *et al.* prepared the noble-metal-free photocatalyst CuS/Cd_{0.3}Zn_{0.7}S and found that the photocatalytic activity reached as high as 3520 $\mu\text{mol g}^{-1} \text{h}^{-1}$.²⁸ Markovskaya *et al.* also synthesized Cd_{0.3}Zn_{0.7}S nanoparticles with Cu_xS and Cu⁰ as co-catalysts, which achieved a photocatalytic hydrogen evolution of 6.4 mmol $\text{g}^{-1} \text{h}^{-1}$.²⁹ Chen *et al.* presented well-defined Cu_{1.94}S–Zn_xCd_{1–x}S heteronanorods for photocatalytic hydrogen evolution, which showed a hydrogen production activity of 7735 $\mu\text{mol g}^{-1} \text{h}^{-1}$.³⁰ Benefiting from the excellent optical performance and matched band gap of CuS, we fabricated a II-type CdS/CuS composite through a hydrothermal method in one step. We have described the growth mechanism, optical properties and H₂ evolution reaction of CdS/CuS composites with different molar ratios of Cd : Cu. Compared with pure CdS, the CdS/CuS composite exhibited better photocatalytic efficiency for H₂ evolution and generated H₂ at a rate of 295 $\mu\text{mol g}^{-1} \text{h}^{-1}$ when the molar ratio of Cd : Cu was 0.5 : 0.5. Thus, CuS plays an important role in improving the photocatalytic activity.

2. Experimental

2.1 Synthesis of CdS, CuS, and CdS/CuS composite

All the chemicals used in this work were of analytical reagent grade. Cadmium nitrate (Cd(NO₃)₂·4H₂O), cupric nitrate (Cu(NO₃)₂·3H₂O), and thiourea were used without any further purification. The aqueous solutions were made using deionized water.

Scheme 1: first, 0.008 mol Cd(NO₃)₂·4H₂O and 0.002 mol Cu(NO₃)₂·3H₂O were added into a beaker containing 90 mL deionized water with stirring for 10 minutes. Then, we added 0.032 mol thiourea into the aqueous solution (Cd : S = 1 : 3, Cu : S = 1 : 4, molar ratio). After stirring for 10 minutes, the aforementioned solution was transferred to a Teflon-lined autoclave of 120 mL capacity.

Scheme 2: first, 0.002 mol Cu(NO₃)₂·3H₂O and 0.02 mol thiourea were added into a beaker containing 90 mL deionized water with stirring for 10 minutes. Then, we added 0.008 mol Cd(NO₃)₂·4H₂O into the aqueous solution. After stirring for 10 minutes, the aforementioned solution was transferred to a Teflon-lined autoclave of 120 mL capacity. The amount of thiourea was fixed at 0.02 mol.

Scheme 3: first, 0.008 mol Cd(NO₃)₂·4H₂O and 0.02 mol thiourea were added into a beaker containing 90 mL deionized water with stirring for 10 minutes. Then, we added 0.002 mol Cu(NO₃)₂·3H₂O into the aqueous solution. After stirring for 10 minutes, the aforementioned solution was transferred into a Teflon-lined autoclave of 120 mL capacity. The amount of thiourea was again fixed at 0.02 mol.

All the autoclaves were sealed and maintained at 160 °C for 24 h. Afterwards, the autoclaves were cooled to room temperature naturally. The resulting products were repeatedly washed with deionized water and absolute ethanol several times.

Finally, the final products were dried at 60 °C in air. We varied the concentration of cupric nitrate (Cd²⁺ : Cu²⁺ = 0.6 : 0.4, 0.5 : 0.5, 0.4 : 0.6, 0.2 : 0.8, molar ratio) to synthesize the CdS/CuS composites. For the purpose of comparison, the pure CdS and CuS were prepared under the same conditions.

2.2 Characterization

The crystal phases of CdS, CuS, and CdS/CuS were measured by powder X-ray diffraction (PXRD, D8-Focus, Bruker AXS) with Ni-filtered and Cu K α radiation ($\lambda = 1.5406 \text{ \AA}$). The morphologies of the as-prepared samples were characterized by field emission scanning electron microscopy (FESEM, SU8010, HITACHI). A scanning electron microscope (SEM, Coxem EM-30AX PLUS⁺) equipped with an energy dispersive spectrometer (EDS, Bruker Nano Xflash610-H) was used to analyze the chemical composition at the sample surface. The optical absorption and room temperature photoluminescence spectra (PL) of the samples were obtained on an ultraviolet-visible spectrophotometer (UV-Vis, UV-2600, Shimadzu) and a fluorescence spectrophotometer (F-4500, HITACHI) equipped with a Xe lamp (excitation wavelength is 338 nm).

2.3 Photocatalytic H₂ evolution

Photocatalytic H₂ evolution was performed in a quartz reactor under visible light irradiation. 0.1 g sample was dispersed in 90 mL DI water in a quartz reactor, and then 10 mL triethanolamine and 1 mL H₂PtCl₆ aqueous solution were added into the aqueous solution under stirring. In this process, triethanolamine was added as a sacrificial electron donor, and H₂PtCl₆ was added to reduce Pt as a cocatalyst. After that, the quartz reactor was purged with N₂ for 15 min to remove air and sealed with a rubber stopper. The Pt cocatalyst was reduced by H₂PtCl₆ under irradiation for 1 h with visible light. Finally, the photocatalytic water splitting reaction was irradiated under the same visible light. The H₂ content was analyzed by a gas chromatograph at a rate of 1 mL gas each hour.

3. Results and discussion

3.1 FESEM results of CdS, CuS and CdS/CuS composite

Fig. 1 shows the FESEM images of CdS and CuS. We can see from Fig. 1 that the morphology of CdS is a flower-like structure, assembled by nanoparticles. The diameter of the flower-like CdS is about 5 μm . The morphology of CuS is also a flower-like structure assembled by nanosheets, with a diameter of about 2 μm . This means that both CdS and CuS are flower-like structures.

Fig. 2 shows the FESEM images of the CdS/CuS composite, synthesized through Scheme 1, at different molar ratios of Cd : Cu. As shown in Fig. 2, the CdS/CuS composites are flower-like structures with different molar ratios of Cd : Cu. The nanoparticles are composed of CdS, and the nanosheets are composed of CuS. When the Cu source is increased, the flower-like structure becomes increasingly assembled by nanosheets.

Fig. 3 shows the FESEM images of the CdS/CuS composite, synthesized through Scheme 2. Fig. 3 shows that the flower-like



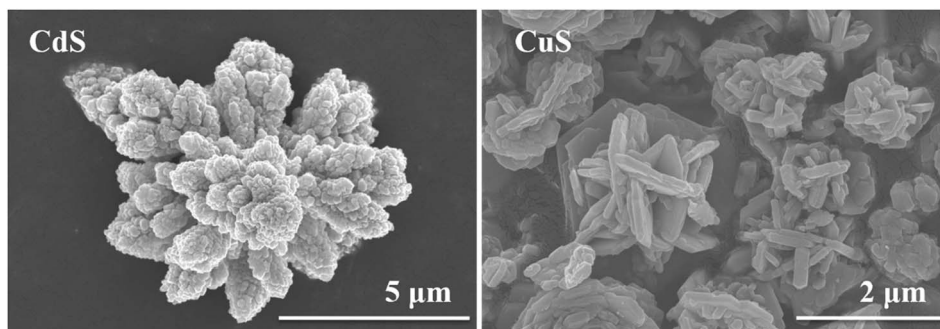


Fig. 1 FESEM images of CdS and CuS.

CdS/CuS composites are mainly assembled by nanosheets with different molar ratios of Cd : Cu using Scheme 2. The amount of the Cu source did not obviously affect the morphologies of the CdS/CuS composites as the molar ratios of Cd : Cu increased.

Fig. 4 shows the FESEM images of the CdS/CuS composite, synthesized through Scheme 3. We can see from Fig. 4 that the morphologies of the CdS/CuS composites are mainly assembled by nanoparticles at high molar ratios of the Cd source. However, when the amount of the Cu source is increased, the flower-like structure becomes increasingly assembled by nanosheets.

In Scheme 1, a Cd source and Cu source were combined in a beaker, with an amount of thiourea that was sufficient for Cd^{2+} and Cu^{2+} to form a strong ligand compound. The CdS/CuS composites were mainly assembled by nanoparticles and nanosheets with low amounts of the Cu source, and the composites were mainly assembled by nanosheets with high amounts of the Cu source. In Scheme 2, the Cu source and thiourea were first added to the beaker; thus, Cu^{2+} may firstly form a strong ligand compound with thiourea. As the stability of Cu ligand compound is stronger than that of the Cd ligand compound, the CdS/CuS composites were mainly assembled by nanosheets with limited amounts of thiourea at different molar ratios of Cd : Cu. In Scheme 3, the Cd source and

thiourea were first added into the beaker; thus, Cd^{2+} may firstly form a ligand compound with thiourea. The CdS/CuS composites were mainly assembled by nanoparticles with high molar ratios of the Cd source. According to the FESEM results shown in Fig. 2 to Fig. 4, we chose the as-prepared samples from Scheme 3 for characterization by XRD, EDS, UV-Vis, PL and H_2 evolution analyses.

3.2 XRD results of CdS, CuS and CdS/CuS composite

Fig. 5 displays the XRD patterns of CdS, CuS and the CdS/CuS composite at different molar ratios of Cd : Cu before and after photocatalytic H_2 evolution. Fig. 5A shows that the diffraction peaks of CdS and CuS were well-indexed to the hexagonal phase of CdS (JSPDS card no. 41-1049) and the hexagonal phase of CuS (JSPDS card no. 06-0464). No peaks belonging to any other phases or impurities were detected. When the molar ratio of Cd : Cu was 0.8 : 0.2, the mixed peaks were attributed to CdS and CuS. The diffraction peaks belonged to CuS when 2θ was 29.2° , 31.7° , and 32.8° . When the molar ratio of Cd : Cu was 0.6 : 0.4, we can find the peak attributed to CuS at $2\theta = 59.2^\circ$. When the molar ratio of Cd : Cu was 0.5 : 0.5, we can find the peak belonging to CuS at $2\theta = 10.7^\circ$. Furthermore, the

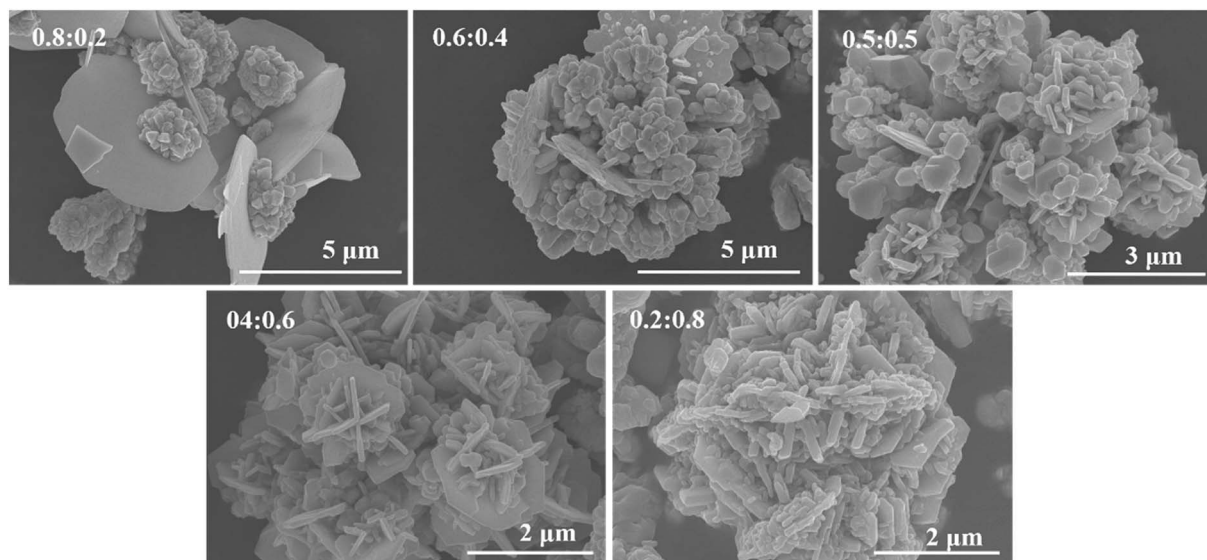


Fig. 2 FESEM images of CdS/CuS composite at different ratios of Cd : Cu through Scheme 1.



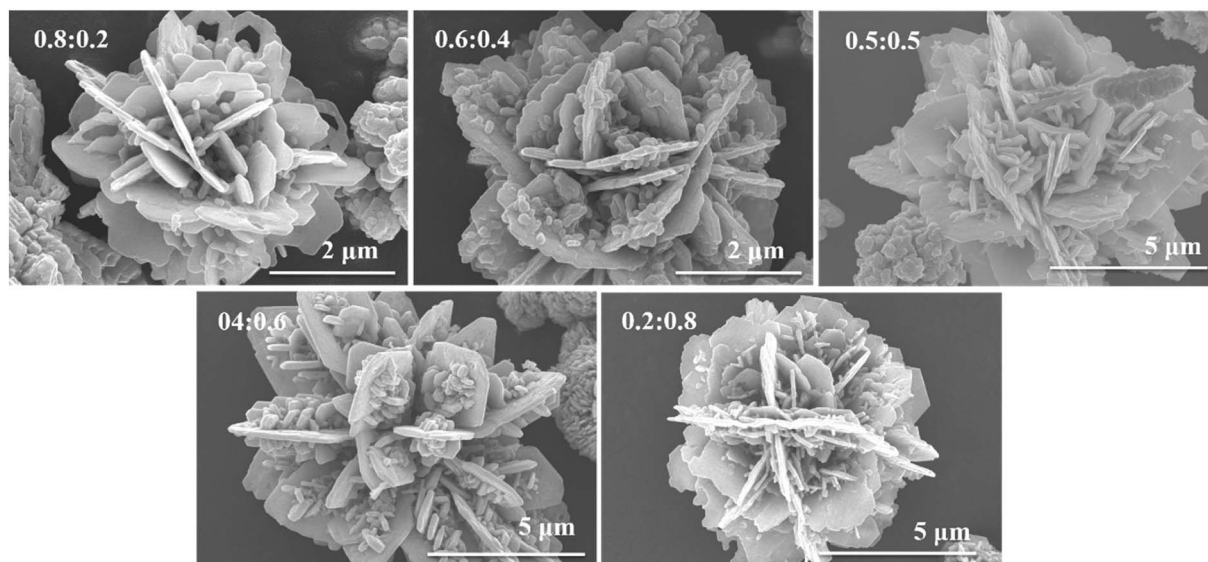


Fig. 3 FESEM images of CdS/CuS composite at different ratios of Cd : Cu through Scheme 2.

intensity of the diffraction peaks belonging to CuS increased when the molar ratios of Cd : Cu changed from 0.8 : 0.2 to 0.2 : 0.8. The diffraction peak at $2\theta = 47.9^\circ$ belongs to CdS and CuS, and the intensity of this diffraction peak also increased with the change in the molar ratios of Cd : Cu. On the other hand, the intensity of some diffraction peaks belonging to CdS decreased at different molar ratios of Cd : Cu. Therefore, we confirmed that we successfully synthesized the CdS/CuS composite based on the XRD results. In addition, the samples exhibit stable photocatalytic activity for H_2 evolution. Fig. 5B shows a small difference in the XRD patterns after the H_2 evolution test, which implies that the CdS, CuS and CdS/CuS samples exhibit excellent stability for H_2 evolution under visible light irradiation.

3.3 EDS results of CdS, CuS and CdS/CuS composite

Fig. 6 presents the EDS results for CdS, CuS and the CdS/CuS composite when the molar ratio of Cd : Cu is 0.5 : 0.5, synthesized following Scheme 3. We can see from Fig. 6A that the elemental composition calculated using EDS analysis was 23 and 77 wt% of S and Cd, respectively, and the atomic ratio of S : Cd was about 1 : 1. Shown in Fig. 6B, the elemental composition calculated by EDS was 36 and 64 wt% of S and Cu, respectively, with an atomic ratio of S : Cu that was about 1 : 1. These results show that the samples contained pure CdS and CuS. As shown in Fig. 6C, the elemental composition was 28, 28, 44 wt% of S, Cu, Cd, respectively, calculated using EDS analysis, with the atomic ratio of S : Cd, S : Cu of about 1 : 1. Therefore, the composites are composed of CdS and CuS. Fig. 7 shows the EDS mapping results of the CdS/CuS composite when the molar

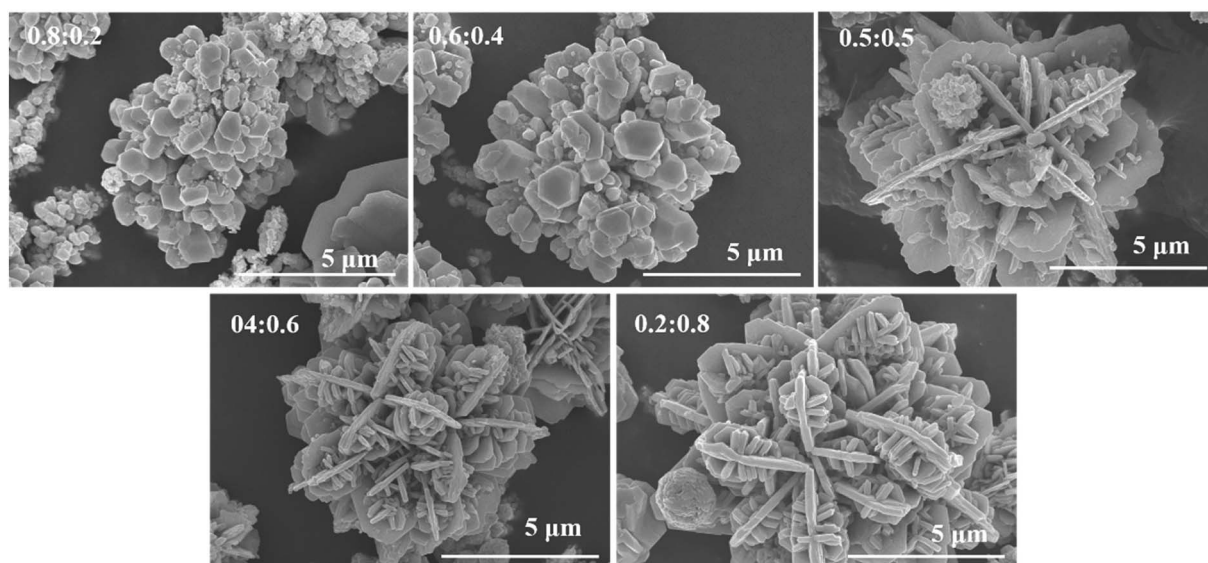


Fig. 4 FESEM images of CdS/CuS composite at different ratios of Cd : Cu through Scheme 3.



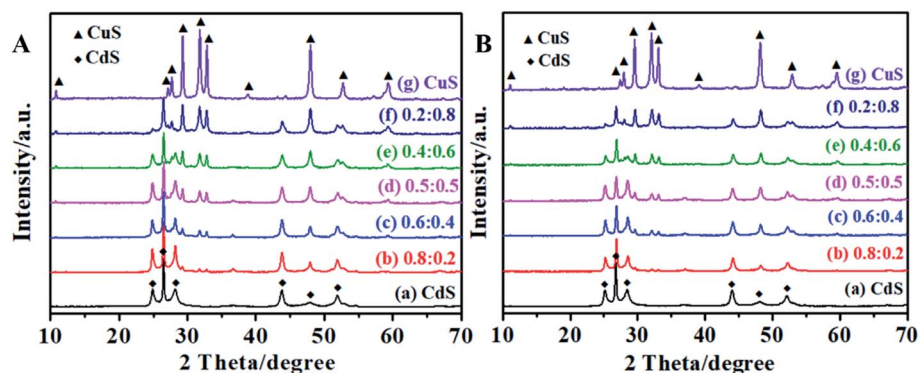


Fig. 5 XRD patterns of CdS, CuS and CdS/CuS composite at different ratios of Cd : Cu. (A) Before photocatalysis. (B) After photocatalysis.

ratio of Cd : Cu was 0.5 : 0.5, synthesized following Scheme 3. We can see from Fig. 7 that the elemental composition of the CdS/CuS composite includes Cd, Cu, and S elements. The nanoparticles belong to the Cd element and the nanosheets belong to the Cu element. Therefore, we confirm that we have successfully synthesized the CdS/CuS composite from EDS results.

3.4 UV-Vis and PL tests of CdS, CuS and CdS/CuS composite

Fig. 8 presents the UV-Vis absorption spectra and PL spectra for CdS, CuS and the CdS/CuS composite at different ratios of Cd : Cu. It can be seen from Fig. 8A that the flower-like CdS structure strongly absorbs in the visible light region upto

520 nm. The flower-like CuS structure showed a strong absorption peak at 620 nm. When CdS and CuS form the CdS/CuS composite, the absorption edge shifts toward longer wavelengths because of the contribution from CuS, which has an absorption peak at 620 nm. Thus, the absorption edge of the CdS/CuS composite shifts toward a wavelength of about 600 nm when the amount of Cu source is increased. Therefore, forming the heterojunction structure with CuS can be used to improve the absorption capability of CdS for visible light. Fig. 8B shows the PL spectra of CdS, CuS and the CdS/CuS composite at different molar ratios. We can see from Fig. 8B that all the samples have a similar emission peak at 370 nm, and the flower-like CdS has another wide emission peak at 582 nm. With the

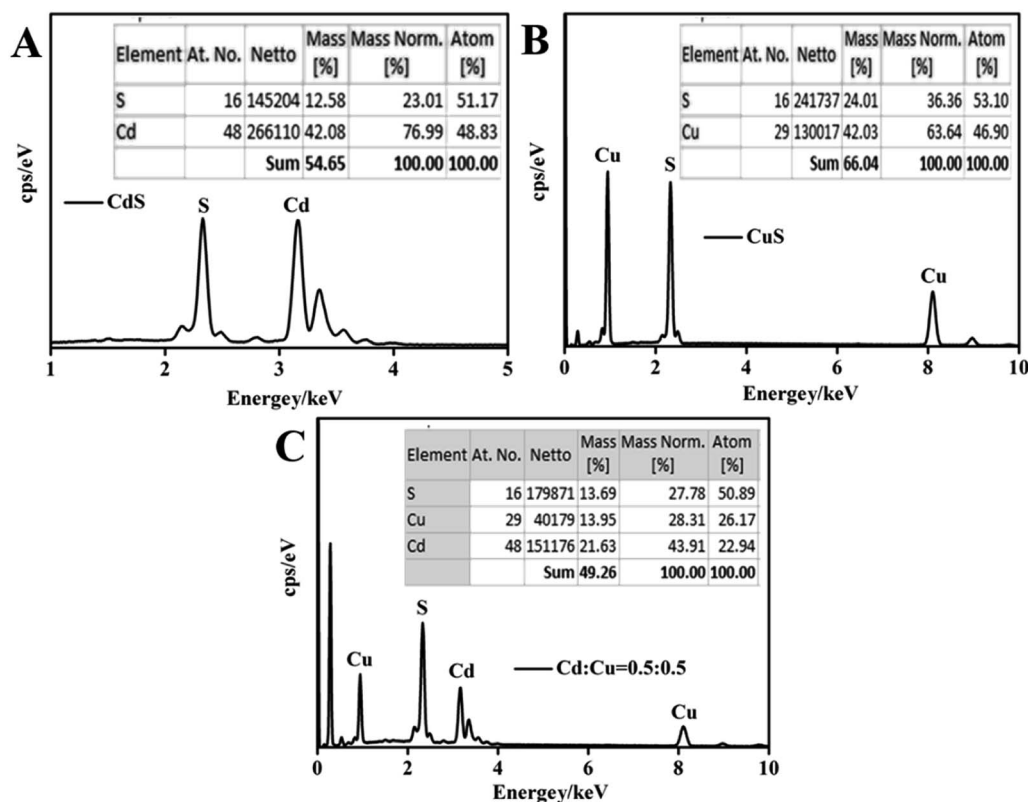


Fig. 6 EDS analysis of CdS, CuS and CdS/CuS composite.



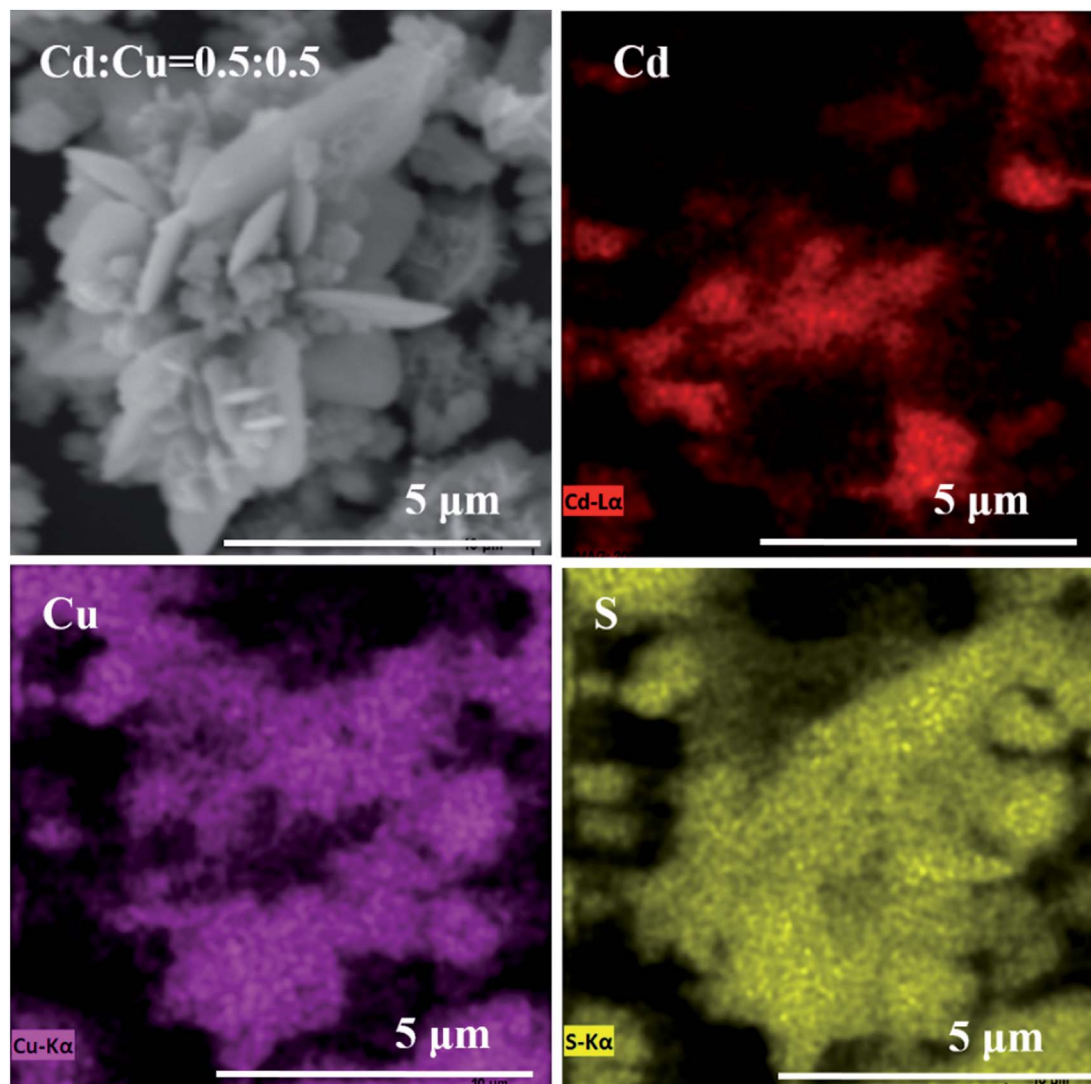


Fig. 7 EDS mapping of CdS/CuS composite when the molar ratio of Cd : Cu is 0.5 : 0.5.

increase in the amount of Cu source, the peak near 582 nm disappears. The possible cause is that the composites have a CuS composition. As we know, PL spectra reveal the efficiency of charge carrier trapping, immigration and transfer.³¹ Thus, the decreased intensity of the PL spectra indicate the lower

recombination rate of the photogenerated electrons and holes, leading to higher photocatalytic activity. Therefore, we can confirm based on Fig. 8 that the formation of a heterojunction structure with CuS can be used to control the optical properties of CdS.

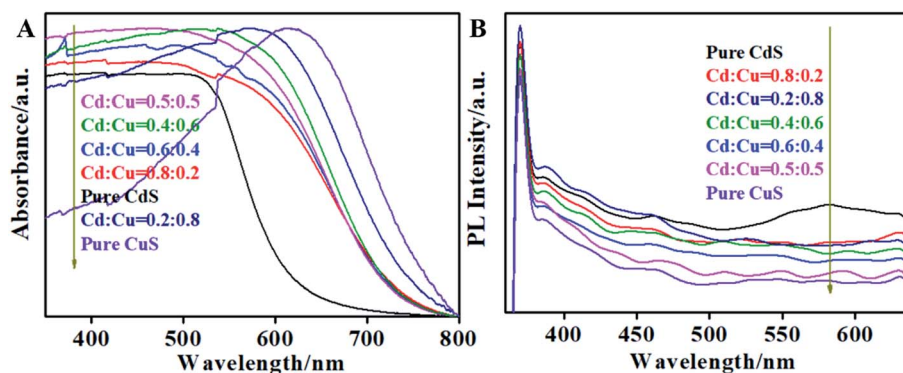


Fig. 8 (A) UV-Vis absorption spectra, (B) PL spectra of CdS, CuS and CdS/CuS composite at different ratios of Cd : Cu.



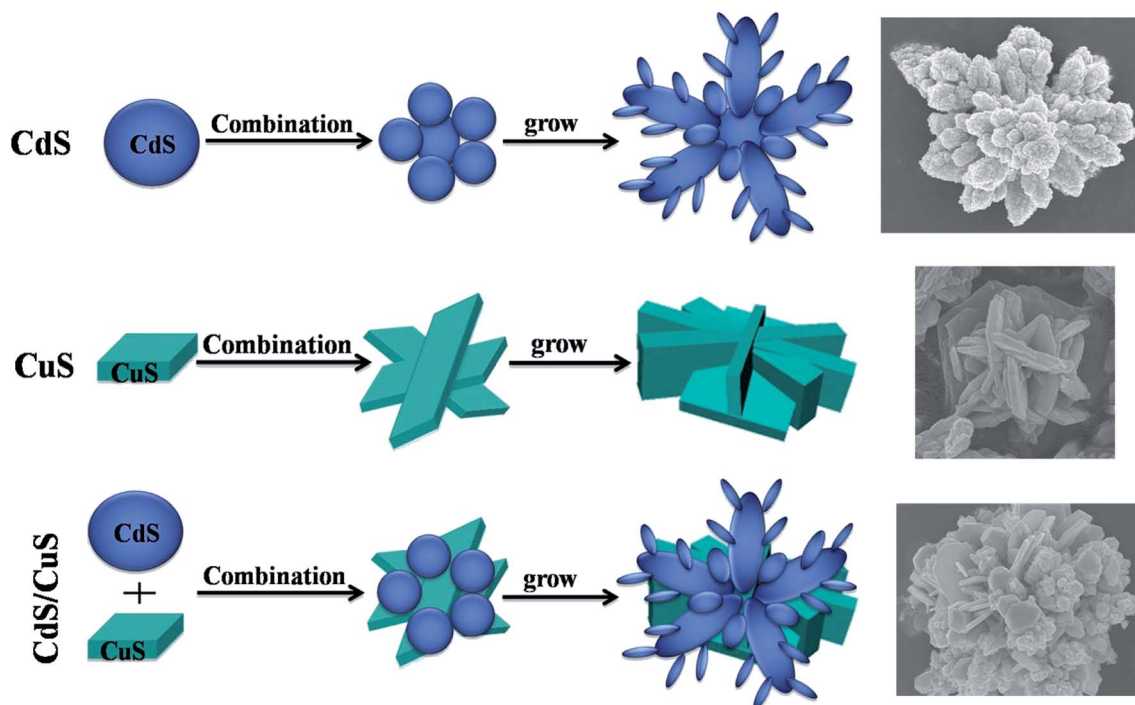


Fig. 9 Growth mechanism of CdS, CuS and CdS/CuS composite.

3.5 Growth mechanism of CdS, CuS and CdS/CuS composite

Fig. 9 shows the growth mechanism of CdS, CuS and the CdS/CuS composite. For CdS, Cd^{2+} and thiourea formed a strong Cd–thiourea ligand compound; Cd^{2+} and S^{2-} were then slowly released and formed CdS nanoparticles. Additionally, the anisotropy of CdS would increase. Several CdS nanoparticles assembled together to form flower-like structures.³² For CuS, Cu^{2+} and thiourea formed a Cu–thiourea ligand compound, and then, the ligand compound released Cu^{2+} and S^{2-} slowly and formed CuS nanosheets upon heating. Then, several CuS nanosheets assembled together to form flower-like structures. For the CdS/CuS composite, Cd^{2+} and Cu^{2+} each formed a strong ligand compound with thiourea. After heating at a high temperature, the ligand compounds slowly released Cu^{2+} , Cd^{2+} and S^{2-} , which formed CdS nanoparticles and CuS nanosheets.³³ On account of the limited thiourea, Cu^{2+} and Cd^{2+}

share the thiourea, which releases S^{2-} . Then, CdS nanoparticles and CuS nanosheets assemble to form a flower-like composite. Therefore, we can fabricate flower-like CdS/CuS composites in one step through a hydrothermal method.

3.6 Photocatalytic H_2 evolution of CdS, CuS and CdS/CuS composite

The visible light photocatalytic H_2 evolution reaction (HER) of CdS, CuS and the CdS/CuS composite is shown in Fig. 10A. The results show that all the samples perform H_2 evolution because CdS and CuS have absorption in the visible light region. We can see from Fig. 10A that pure CdS and pure CuS each generate H_2 at rates of $207 \mu\text{mol g}^{-1} \text{h}^{-1}$ and $219 \mu\text{mol g}^{-1} \text{h}^{-1}$, respectively. After we synthesized the CdS/CuS composites with different ratios of Cd : Cu, the increased efficiency of the H_2 production compared to that of pure CdS or pure CuS becomes evident.

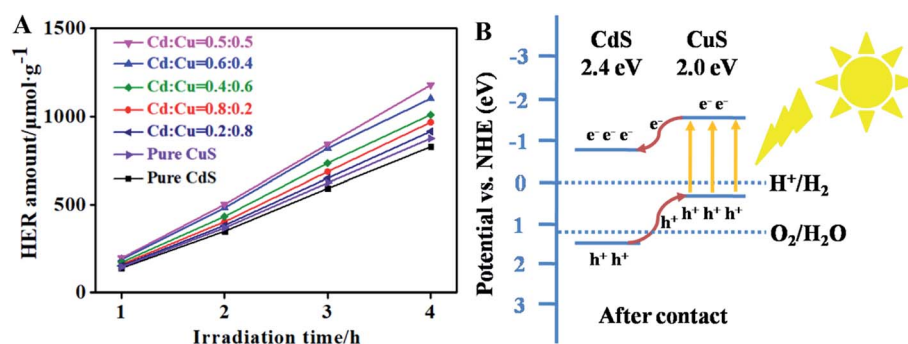


Fig. 10 (A) Time courses of H_2 evolution with CdS, CuS and CdS/CuS composite, (B) schematic diagram of electronic transfer mechanism.



When the ratio of Cd : Cu is 0.5 : 0.5, the CdS/CuS composites generate H₂ at a rate of 295 $\mu\text{mol g}^{-1} \text{h}^{-1}$, which benefits from the constructed CdS/CuS heterojunction. The increase in the size of the CdS/CuS composite did not obviously increase the efficiency of H₂ production. These results show that the micro-sized CdS/CuS composite could be synthesized as nanosized to further enhance H₂ production because of nanosized materials have larger specific surface. As is shown in Fig. 10B, when CuS combines with CdS to construct a II-type heterojunction, the visible light-excited electrons in the conduction band (CB) of CuS can transfer into the CB of CdS, and the holes in the valence band (VB) of CdS can transfer into the VB of CuS, which can enhance the separation of the photoinduced charge carriers and holes.^{34,35} In this way, the efficient separation of photo-generated electron-hole pairs can be achieved, which further improves the visible light photocatalytic H₂ evolution activity. Therefore, forming heterojunction structure with CuS can be used to enhance H₂ production of CdS.

4. Conclusions

In summary, we have synthesized a CdS/CuS composite through a hydrothermal method in one step. FESEM images show a flower-like morphology for CdS, CuS and the CdS/CuS composite synthesized following different schemes. EDS results also confirm that all the composites are composed of CdS and CuS. XRD results show that pure CdS and pure CuS are in the hexagonal phase, and the CdS/CuS composites have diffraction peaks belonging to CdS and CuS with different ratios of Cd : Cu. UV-Vis and PL spectroscopy results show that forming a heterojunction structure with CuS can be used to control the optical properties of CdS. H₂ evolution results show that the CdS/CuS composite generates H₂ at a rate of 295 $\mu\text{mol g}^{-1} \text{h}^{-1}$, which is higher than that of pure CdS. Therefore, forming a heterojunction structure with CuS can be used to enhance the H₂ production of CdS.

Funding information

This work was supported by the National Natural Science Foundation of China (No. 41472042 and 41172051), Guangdong Provincial Key Laboratory of Soil and Groundwater Pollution Control (No. 2017B030301012), Open Research Topic for Engineering Research Center of Nano-Geomaterials of Ministry of Education of China University of Geosciences (No. NGM2018KF019), the financial support was gratefully appreciated.

Conflicts of interest

There are no conflicts to declare.

References

- 1 H. Yang, Z. L. Jin, D. D. Liu, K. Fan and G. R. Wang, Visible Light Harvesting and Spatial Charge Separation over the Creative Ni/CdS/Co₃O₄ Photocatalyst, *J. Phys. Chem. C*, 2018, **122**, 10430–10441.
- 2 A. Fujishima and K. Honda, Electrochemical Photocatalysis of Water at a Semiconductor Electrode, *Nature*, 1972, **238**, 37–38.
- 3 Q. Li, B. D. Guo, J. G. Yu, J. R. Ran, B. H. Zhang, H. J. Yan and J. R. Gong, Highly Efficient Visible-Light-Driven Photocatalytic Hydrogen Production of CdS-Cluster-Decorated Graphene Nanosheets, *J. Am. Chem. Soc.*, 2011, **133**, 10878–10884.
- 4 H. Tong, S. X. Ouyang, Y. P. Bi, N. T. Umezawa, M. Oshikiri and J. H. Ye, Nano-Photocatalytic Materials: Possibilities and Challenges, *Adv. Mater.*, 2012, **24**, 229–251.
- 5 Y. C. Li, Q. Ma, J. Han, L. L. Ji, J. X. Wang, J. Y. Chen and Y. Q. Wang, Controllable Preparation, Growth Mechanism and the Properties Research of TiO₂ Nanotube Arrays, *Appl. Surf. Sci.*, 2014, **297**, 103–108.
- 6 Y. Q. Wang, Q. Ma, H. X. Jia and Z. S. Wang, One-Step Solution Synthesis and Formation Mechanism of Flower-like ZnO and its Structural and Optical Characterization, *Ceram. Int.*, 2016, **42**, 10751–10757.
- 7 G. G. Zhang, Z. A. Lan, L. H. Lin, S. Lin and X. C. Wang, Overall Water Splitting by Pt/g-C₃N₄ Photocatalysts without Using Sacrificial Agents, *Chem. Sci.*, 2016, **7**, 3062–3066.
- 8 Q. W. Tian, M. H. Tang, Y. G. Sun, R. J. Zou, Z. G. Chen, M. F. Zhu, S. P. Yang, J. L. Wang, J. H. Wang and J. Q. Hu, Hydrophilic Flower-Like CuS Superstructures as an Efficient 980 nm Laser-Driven Photothermal Agent for Ablation of Cancer Cells, *Adv. Mater.*, 2011, **23**, 3542–3547.
- 9 L. G. Xia, J. Bai, J. H. Li, Q. Y. Zeng, X. J. Li and B. X. Zhou, A Highly Efficient BiVO₄/WO₃/W Heterojunction Photoanode for Visible-Light Responsive Dual Photoelectrode Photocatalytic Fuel Cell, *Appl. Catal., B*, 2016, **183**, 224–230.
- 10 H. L. Li, K. Yu, X. Lei, B. J. Guo, H. Fu and Z. Q. Zhu, Hydrothermal Synthesis of Novel MoS₂/BiVO₄ Hetero-Nanoflowers with Enhanced Photocatalytic Activity and a Mechanism Investigation, *J. Phys. Chem. C*, 2015, **119**, 22681–22689.
- 11 L. Vayssieres, Growth of Arrayed Nanorods and Nanowires of ZnO from Aqueous Solutions, *Adv. Mater.*, 2003, **15**, 464–466.
- 12 J. B. Shi, G. Q. Chen, G. M. Zeng, A. W. Chen, K. He, Z. Z. Huang, L. Hu, J. W. Zeng, J. Wu and W. W. Liu, Hydrothermal Synthesis of Graphene Wrapped Fe-doped TiO₂ Nanospheres with High Photocatalysis Performance, *Ceram. Int.*, 2018, **44**, 7473–7480.
- 13 Z. Li, Z. Zhou, J. W. Ma, Y. Li, W. C. Peng, G. L. Zhang, F. B. Zhang and X. B. Fan, Hierarchical Photocatalyst of In₂S₃ on Exfoliated MoS₂ Nanosheets for Enhanced Visible-Light-Driven Aza-Henry Reaction, *Appl. Catal., B*, 2018, **237**, 288–294.
- 14 Z. Yu, F. Y. Qu and X. Wu, Dendritic CdS Assemblies for Removal of Organic Dye Molecules, *Dalton Trans.*, 2014, **43**, 4847–4853.
- 15 J. Z. Chen, X. J. Wu, L. S. Yin, B. Li, X. Hong, Z. X. Fan, B. Chen, C. Xue and H. Zhang, One-pot Synthesis of CdS Nanocrystals Hybridized with Single-Layer Transition-Metal Dichalcogenide Nanosheets for Efficient Photocatalytic



- Hydrogen Evolution, *Angew. Chem., Int. Ed.*, 2015, **54**, 1210–1214.
- 16 C. Z. Wang, Y. F. E, L. Z. Fan, Z. H. Wang, H. B. Liu, Y. L. Li, S. H. Yang and Y. L. Li, Directed Assembly of Hierarchical CdS Nanotube Arrays from CdS Nanoparticles: Enhanced Solid-State Electrochemiluminescence in H_2O_2 Solution, *Adv. Mater.*, 2010, **19**, 3677–3681.
 - 17 Q. Li, B. D. Guo, J. G. Yu, J. R. Ran and B. H. Zhang, Highly Efficient Visible-Light-Driven Photocatalytic Hydrogen Production of CdS-Cluster-Decorated Graphene Nanosheets, *J. Am. Chem. Soc.*, 2011, **133**, 10878–10884.
 - 18 N. Zhang, S. Liu, X. Fu and Y. J. Xu, Fabrication of Coenocytic Pd@CdS Nanocomposite as a Visible Light Photocatalyst for Selective Transformation under Mild Conditions, *J. Mater. Chem.*, 2012, **22**, 5042–5052.
 - 19 W. Jiang, Y. Liu, R. Zong, Z. Li, W. Yao and Y. Zhu, Photocatalytic Hydrogen Generation on Bifunctional Ternary Heterostructured $\text{In}_2\text{S}_3/\text{MoS}_2/\text{CdS}$ Composites with High Activity and Stability under Visible Light Irradiation, *J. Mater. Chem. A*, 2015, **3**, 18406–18412.
 - 20 Z. Han, F. Qiu, R. Eisenberg, P. L. Holland and T. D. Krauss, Robust Photogeneration of H_2 in Water Using Semiconductor Nanocrystals and a Nickel Catalyst, *Science*, 2012, **338**, 1321–1324.
 - 21 P. Wang, Y. Sheng, F. Wang and H. Yu, Synergistic Effect of Electron-Transfer Mediator and Interfacial Catalytic Active-Site for the Enhanced H_2 -Evolution Performance: A Case Study of CdS-Au Photocatalyst, *Appl. Catal., B*, 2018, **220**, 561–569.
 - 22 H. Yu, X. Huang, P. Wang and J. Yu, Enhanced Photoinduced-Stability and Photocatalytic Activity of CdS by Dual Amorphous Cocatalysts: Synergistic Effect of Ti(IV)-Hole Cocatalyst and Ni(II)-Electron Cocatalyst, *J. Phys. Chem. C*, 2016, **120**, 3722–3730.
 - 23 G. S. Thool, K. Sraveen, A. K. Singh, U. Pal and S. P. Singh, Cowrie-Shell Architectures: Low Temperature Growth of Ni Doped CdS Film, *J. Alloys Compd.*, 2015, **649**, 553–558.
 - 24 D. W. Wakerley, M. F. Kuehnle, K. L. Orchard, K. H. Ly, T. E. Rosser and E. Reisner, Solar-Driven Reforming of Lignocellulose to H_2 with a CdS/CdO_x Photocatalyst, *Nat. Energy*, 2017, **2**, 17021.
 - 25 L. Chen, D. W. Meng, X. L. Wu, A. Q. Wang, J. X. Wang, Y. Q. Wang and M. H. Yu, In Situ Synthesis of V^{4+} and Ce^{3+} Self-Doped $\text{BiVO}_4/\text{CeO}_2$ Heterostructured Nanocomposites with High Surface Areas and Enhanced Visible-Light Photocatalytic Activity, *J. Phys. Chem. C*, 2016, **120**, 18548–18559.
 - 26 H. Zhu and T. Lian, Wavefunction Engineering in Quantum Confined Semiconductor Nanoheterostructures for Efficient Charge Separation and Solar Energy Conversion, *Energy Environ. Sci.*, 2012, **5**, 9406–9418.
 - 27 P. P. Wang, Y. H. Gao, P. J. Li, X. F. Zhang, H. L. Niu and Z. Zheng, Doping Zn^{2+} in CuS Nanoflowers into Chemically Homogeneous $\text{Zn}_{0.49}\text{Cu}_{0.50}\text{S}_{1.01}$ Superlattice Crystal Structure as High-Efficiency n-Type Photoelectric Semiconductors, *ACS Appl. Mater. Interfaces*, 2016, **8**, 15820–15827.
 - 28 D. V. Markovskaya, S. V. Cherepanova, A. A. Saraev, E. Y. Gerasimov and E. A. Kozlova, Photocatalytic hydrogen evolution from aqueous solutions of $\text{Na}_2\text{S}/\text{Na}_2\text{SO}_3$ under visible light irradiation on CuS/ $\text{Cd}_{0.3}\text{Zn}_{0.7}\text{S}$ and $\text{Ni}_2\text{Cd}_{0.3}\text{Zn}_{0.7}\text{S}_{1+z}$, *Chem. Eng. J.*, 2015, **262**, 146–155.
 - 29 D. V. Markovskaya, E. A. Kozlova, O. A. Stonkus, A. A. Saraev, S. V. Cherepanova and V. N. Parmon, Evolution of the state of copper-based co-catalysts of the $\text{Cd}_{0.3}\text{Zn}_{0.7}\text{S}$ photocatalyst at the photoproduction of hydrogen under action of visible light, *Int. J. Hydrogen Energy*, 2017, **42**, 30067–30075.
 - 30 Y. G. Chen, S. Zhao, X. Wang, Q. Peng, R. Lin, Y. Wang, R. G. Shen, X. Cao, L. B. Zhang, G. Zhou, J. Li, A. D. Xia and Y. D. Li, Synergetic integration of $\text{Cu}_{1.94}\text{S}-\text{Zn}_x\text{Cd}_{1-x}\text{S}$ heteronanorods for enhanced visible-light-driven photocatalytic hydrogen production, *J. Am. Chem. Soc.*, 2016, **138**, 4286–4289.
 - 31 J. H. Yang, R. J. Liu, S. Huang, Y. Shao, Y. Huang and Y. Yu, Enhanced photocatalytic activity and stability of interstitial Ga-doped CdS: combination of experiment and calculation, *Catal. Today*, 2014, **224**, 104–113.
 - 32 Y. Q. Wang, X. D. Yang, Q. Ma, J. H. Kong, H. X. Jia, Z. S. Wang and M. H. Yu, Preparation of Flower-Like CdS with SDBS as Surfactant by Hydrothermal Method and Its Optical Properties, *Appl. Surf. Sci.*, 2015, **340**, 18–24.
 - 33 X. S. Hu, Y. Shen, L. H. Xu, L. M. Wang, L. S. Lu and Y. T. Zhang, Preparation of Flower-Like CuS by Solvothermal Method for Photocatalytic, UV Protection and EMI Shielding Applications, *Appl. Surf. Sci.*, 2016, **385**, 162–170.
 - 34 B. Kim, K. Kim, Y. Kwon, W. Lee, W. H. Shin, S. Kim and J. Bang, $\text{CuInS}_2/\text{CdS}$ -Heterostructured Nanotetrapods by Seeded Growth and their Photovoltaic Properties, *ACS Appl. Nano Mater.*, 2018, **1**, 2449–2454.
 - 35 D. Y. Hong, W. L. Zang, X. Guo, Y. M. Fu, H. X. He, J. Sun, L. L. Xing, B. D. Liu and X. Y. Xue, High Piezo-Photocatalytic Efficiency of CuS/ZnO Nanowires Using Both Solar and Mechanical Energy for Degrading Organic Dye, *ACS Appl. Mater. Interfaces*, 2016, **8**, 21302–21314.

